JOURNAL OF THERMOPHYSICS AND HEAT TRANSFER
Vol. 8, No. 3, July–Sept. 1994

Nonlinear Dynamics of Laminar Boundary Layers in Pulsatile Stagnation Flows

E. C. Mladin* and D. A. Zumbrunnen†
Clemson University, Clemson, South Carolina 29634

In order to elucidate convective heat transfer in time-varying stagnation flows, a mathematical model was developed to study the nonlinear dynamics of the hydrodynamic and thermal boundary layers within a planar stagnation region to imposed temporal variations in both the freestream velocity and surface heat flux. Such a model has practical utility in the study of heat transfer to gas turbine blades, to experimental work involving pulsatile stagnation flows, and to the development of miniature thermal sensors. Equations are not linearized in order to preserve the influence of nonlinearities on dynamical behavior. As model parameters are varied, dramatically different responses arise due to the influence of nonlinearities. Time-averaged Nusselt numbers decrease with increasing pulse magnitude and are in excellent agreement with experimental results. Interactions between variations in the incident flow velocity and surface heating lead to very complex behavior in the thermal boundary layer, surface temperature, and Nusselt number responses.

Nomenclature

C = steady dimensional freestream velocity gradient, $C_* V_i/w$
C_* = constant dimensionless freestream velocity gradient from potential flow theory, $C_t w/V_i$
C_f = friction coefficient, $\mu \partial u/\partial y|_{y=0}/(\rho V_{i0}^2/2)$
C_{f*} = ratio of instantaneous friction coefficient to steady-state friction coefficient, C_f/C_{f0}
C_t = instantaneous freestream velocity gradient
c_p = specific heat at constant pressure
d = cylinder diameter
f = frequency of imposed sinusoidal incident flow variation
f_* = dimensionless frequency, f/C
f_q = frequency of imposed sinusoidal surface heat flux
f_{q*} = dimensionless frequency, f_q/C
$f_1, f_2, \ldots, f_5$ = functions defined by Eqs. (24–28)
h = heat transfer coefficient
k = thermal conductivity
Nu_* = ratio of instantaneous Nusselt number to steady-state Nusselt number, Nu_w/Nu_{w0}
$Nu_{*,\text{avg}}$ = time-averaged value of Nu_*, Eq. (32)
Nu_w = Nusselt number, hw/k
Pr = Prandtl number
p = instantaneous local static pressure
q_s = surface heat flux
q_{s*} = dimensionless surface heat flux, Eqs. (22) and (34a)
Re_w = Reynolds number, $V_i w/\nu$
Sr_w = Strouhal number, fw/V_i, $f_* C_*$
T = fluid temperature
T_s = surface temperature
T_∞ = freestream temperature
t = time
U_∞ = instantaneous local velocity component parallel to the surface in the freestream
$U_{\infty *}$ = dimensionless freestream velocity, U_∞/V_{i0}
u = local velocity component parallel to the surface and within the hydrodynamic boundary layer
u_* = dimensionless velocity, u/U_∞
V_i = instantaneous incident flow velocity
v = local velocity component perpendicular to the surface and inside the hydrodynamic boundary layer
w = characteristic length scale, jet width or cylinder diameter
x = distance along impingement surface from stagnation line, Fig. 1
x_* = dimensionless distance, x/w
y = distance perpendicular to impingement surface, Fig. 1
β = dimensionless distance, y/Δ
Γ = dimensionless thermal boundary-layer thickness, $C\Delta^2/\nu$
Γ_* = normalized dimensionless thermal boundary-layer thickness, Γ/Γ_0
Δ = instantaneous thermal boundary-layer thickness
δ = instantaneous hydrodynamic boundary-layer thickness
ε_1 = dimensionless peak to mean amplitude for sinusoidal flow variation, Eq. (33)
ε_2 = dimensionless peak to mean amplitude for sinusoidal surface heat flux variation, Eq. (34)
η = dimensionless distance, y/δ
Θ = dimensionless fluid temperature, $(T - T_\infty)/(T_{s0} - T_\infty)$
Θ_s = dimensionless surface temperature, $(T_s - T_\infty)/(T_{s0} - T_\infty)$
Λ = dimensionless hydrodynamic boundary-layer thickness, $C\delta^2/\nu$
Λ_* = normalized dimensionless hydrodynamic boundary-layer thickness, Λ/Λ_0
μ = dynamic viscosity
ν = kinematic viscosity, μ/ρ
ρ = mass density
τ = dimensionless time, Ct
ψ_1, ψ_2, ψ_3 = functions defined by Eqs. (17–19)

Received Feb. 22, 1993; revision received Oct. 14, 1993; accepted for publication Oct. 15, 1993. Copyright © 1993 by the American Institute of Aeronautics and Astronautics, Inc. All rights reserved.

*Graduate Research Assistant, Thermal Sciences Research Laboratory, Department of Mechanical Engineering.
†Associate Professor, Thermal Sciences Research Laboratory, Department of Mechanical Engineering. Member AIAA.

$\Omega, \Omega_1, \Omega_2$ = dimensionless variables defined by Eqs. (13), (16a), and (16b)
ω = function defined by Eq. (14)

Subscript
0 = corresponding to $t = 0$ and to steady-state conditions

Introduction

UNSTEADY flows over heated or cooled bodies are encountered in many engineering applications. Examples include rotor-mounted blades in a gas turbine where flow is periodically renewed in the vicinity of stationary nozzles and miniature thermal sensors used to measure instantaneous flow velocities or convective heat fluxes. In addition, pulsations in an incident flow can be induced to alter the time-averaged heat transfer characteristics of impinging jet flows.[1,2] In all such situations, a stagnation region is formed in which heat transfer rates are often highest. In this study, a detailed mathematical model was developed to investigate the nonlinear dynamics of the hydrodynamic and thermal boundary layers within a planar stagnation region subjected to temporal variations in the freestream velocity and/or surface heat flux. Temporal variations in the surface heat flux are included, because thermal sensors often rely on electronic control circuitry to regulate sensor temperature, and unsteady heat generation may occur in electrically or radiatively heated surfaces and thereby directly influence the thermal boundary-layer response.

Although a planar stagnation flow is considered, this study is related broadly to the emerging field of nonlinear dynamics and chaos. Chaos describes the unpredictable, long-term dynamic behavior of systems which are often amenable to precise mathematical modeling. Responses in such *deterministic* systems are very sensitive to initial conditions, generate nonperiodic bounded solutions, and are comprised of a broad spectrum of frequencies. For chaotic behavior to occur, a governing system of coupled, first-order, ordinary differential equations must consist of at least two equations for the nonautonomous case (i.e., behavior influenced by applied forcing functions), and of at least three equations for the autonomous case (i.e., no external forcing). In addition, the system equations must include nonlinear terms in at least one dependent variable.[3] In this study, nonlinearities are shown to arise when a partial differential equation, which is linear in a dependent variable, is used to obtain a dynamical equation for a related dependent variable. Such *imbedded nonlinearities* demonstrate that complex and possibly chaotic behavior may arise even in situations where it is unexpected.

Several studies have been performed to illustrate chaos in deterministic convective systems. Saltzman[4] and Lorenz[5] employed spectral methods to obtain an autonomous system of three ordinary differential equations representing two-dimensional Rayleigh-Benard convection from the Navier-Stokes and energy equations. Although truncations and basis functions employed in the spectral method constituted significant approximations, the stability of convection cells was substantially clarified and the temperature-dependent body force was shown to lead to chaotic responses for certain combinations of physical parameters. Similar approximate mathematical models have been developed for natural convection in single- or double-thermal convection loops and have been shown to provide good agreement with experiment.[6] Chaos in double-diffusive natural convection has also been considered.[7] Approximate dynamics models may be used to assess the influence of nonlinearities on flow instabilities in boiling heat transfer occurring in water-cooled fuel assemblies of nuclear reactor cores.[8] The aforementioned theoretical analyses can be employed to estimate parametric values which give rise to instabilities and complex or chaotic behavior. Instabilities and chaos may be beneficial in some instances if heat or mass transfer is promoted. Enhanced convective heat transfer due to intermittency in impinging water jet flows[1] was obtained experimentally with guidance from theoretical nonlinear dynamics models.[9] Alternately, if the onset of chaotic behavior signals a breakdown in a desirable condition, engineering systems can be designed such that requisite parameters are not encountered. Theoretical analyses in nonlinear dynamics, although commonly approximate in order to permit tenable computation times, are crucial in the planning of experiments to investigate possible instabilities and chaotic behavior.

Kasza[10] developed a mathematical model to study the thermal response of a two-dimensional, unsteady, laminar, incompressible, constant property boundary layer in the vicinity of a stagnation point. The temperatures of the fluid freestream and surface were assumed to be uniform and not dependent on time. Upon employing power series solutions to the conservation equations for momentum and energy, a system of two ordinary differential equations was obtained for the transient responses of the surface heat flux and wall shear stress. Sinusoidal pulsations in the incident freestream velocity yielded elevated surface heat fluxes. However, the imposed constant surface temperature in conjunction with a varying surface heat flux is physically restrictive and may account for the calculated enhancements. Andraka and Diller[11] performed an experimental investigation of the effects of a sinusoidal variation about a mean flow velocity with magnitudes as high as 25% on the local time-averaged heat transfer in the front stagnation region of a stationary cylinder in an air crossflow with Re_d = 50,000 and Strouhal numbers Sr_d ($=fd/V_i$) less than about 0.24. Time-averaged convective heat transfer was found to be unaffected by the sinusoidal flow variations. No discernible influence on time-averaged heat transfer was measured for the related situation[12] in which a cylinder oscillates in either the flow direction or perpendicular to the flow with $750 < Re_d < 6000$ and $Sr_d < 0.007$. Although some of the aforementioned experimental studies revealed no significant effects on time-averaged heat transfer, it should be noted that only limited combinations of major parameters (e.g., pulse magnitude and frequency, pulse waveform, Prandtl number) have been considered. As will be shown, these limited experimental results are consistent with the model predictions of this study. At higher pulse magnitudes, model predictions and more recent experiments indicate that reductions in time-averaged Nusselt number occur.

The stagnation region which is considered in this study is depicted in Fig. 1. Such flows arise beneath impinging planar or "slot" jets, on a cylinder or sensor filament in a crossflow, or in the front stagnation region of any bluff body, such as gas turbine blades, where the frontal surface can be effectively represented by a tangent plane. Although V_i and the freestream stagnation velocities U_∞ and V_∞ may be unsteady, it is assumed that symmetry in the flow is preserved about the

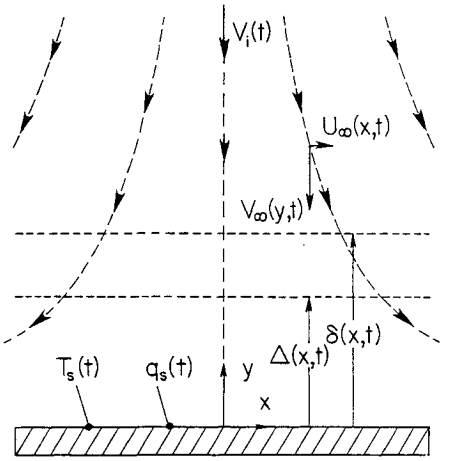

Fig. 1 Unsteady planar stagnation flow on a surface with imposed time-dependent heat flux and incident flow velocity.

stagnation line. The hydrodynamic and thermal boundary layers are thereby spatially constant in the vicinity of $x = 0$. Forcing functions which are selected for the incident flow velocity become identical to those for steady flow beyond the hydrodynamic boundary layer when temporal variations cease. The steady-state velocity components are given by[13]

$$U_\infty = Cx \tag{1a}$$

$$V_\infty = -Cy \tag{1b}$$

where

$$C = C_* V_i / w \tag{1c}$$

A periodic heat flux $q_s(t)$ at the impingement surface ($y = 0$) is specified and the temperature T_∞ is a constant. The velocity gradient C_* depends on the steady flow characteristics and the surface geometry, and can be calculated from potential flow theory or from experimental measurements.[14–16] In the analysis that follows, C_* is found to influence the *dimensional* transient response significantly. Values for some common stagnation flows have been tabulated[9] and may be used to adapt the dimensionless results of this study to a specific application.

Theoretical and experimental studies have shown that the local heat transfer coefficient is spatially constant to within 1% over a distance equal to about one-half jet width from the stagnation line of a laminar planar jet with a uniform fluid discharge velocity across the nozzle width.[14] This uniformity is attributable to the symmetry of the impinging flow (Fig. 1) and extends the validity of this study to regions away from the stagnation line. Laminar flow is assumed so as to provide physical insight into the nature of transient effects and thereby illuminate important phenomena which may be the subject of future experimental work. Such solutions are of direct utility when the characteristic dimension of a cylinder or nozzle, and thereby the associated Reynolds number, is small. Examples include miniature jets which may be used to cool assemblies of microelectronic or micromechanical components, and fine diameter wires or elements employed in various thermal flow or heat flux sensors.

Analysis

Description of Analytical Method and Assumptions

Consideration of transient effects in convection often precludes an exact analytical approach since transient terms that are routinely omitted in many convection studies must be retained. For example, where transient effects can be incorporated with similarity methods, restrictions are often necessary regarding functional relationships between variables.[17] Calculations in this study must be performed over large time intervals to reveal important characteristics due to nonlinearities in the equations governing the transient responses. Direct numerical models to the transient, two-dimensional problem considered here would therefore be extremely time-consuming computationally. A solution methodology was sought which is consistent with approaches used in recent studies of the nonlinear dynamics and chaos of thermal systems and discrete mechanical systems. The responses of such systems are commonly represented by a system of first-order, ordinary differential equations. Where the system response is governed by partial differential equations as in this study, spectral, Galerkin, or perturbation methods[18] are often employed to obtain a corresponding system of first-order, ordinary differential equations.[4–6,19] Approximations are invoked in all cases during the derivation of the resulting systems of equations either by truncating series representations or in selecting basis functions for dependent variables. The approach which was selected is related to the von Karman-Pohlhausen technique. This technique has been widely applied in studies of hydrodynamic boundary layers on airfoils, where the hydrodynamic boundary layer is significantly influenced by a pressure gradient,[13] as in stagnation flows, and was recently extended to transient boundary layers.[9] In the related technique implemented here, equations for momentum and energy conservation in their integral and differential forms are used with *temporally adaptive profiles* for fluid velocity and temperature to obtain governing equations for the hydrodynamic and thermal boundary-layer responses.

The problem was solved under the following general assumptions: 1) incompressible laminar flow, 2) constant thermophysical properties, 3) negligible viscous heating, 4) negligible body forces in comparison to viscous forces, 5) constant T_∞, and 6) $\Delta < \delta$. The last assumption restricts the model to fluids with Prandtl numbers greater than about unity. However, results have been shown in a related study[9] to remain accurate to within 2% for $Pr > 0.7$.

Conservation Equations and Boundary Conditions

Transient boundary-layer equations for momentum conservation in differential and integral forms, which corresponds to the aforementioned assumptions and stagnation flow in Fig. 1, are

$$\frac{\partial u}{\partial t} + u\frac{\partial u}{\partial x} + v\frac{\partial u}{\partial y} = -\frac{1}{\rho}\frac{\partial p}{\partial x} + \nu\frac{\partial^2 u}{\partial y^2} \tag{2}$$

$$\frac{\partial}{\partial t}\int_0^\delta u\,dy - U_\infty\frac{\partial \delta}{\partial t} + \frac{\partial}{\partial x}\int_0^\delta u(u - U_\infty)\,dy + \frac{\partial U_\infty}{\partial x}\int_0^\delta u\,dy = -\frac{1}{\rho}\int_0^\delta \frac{\partial p}{\partial x}\,dy - \nu\left.\frac{\partial u}{\partial y}\right|_{y=0} \tag{3}$$

The associated transient boundary-layer equations for energy conservation, in differential and integral forms, are

$$\rho c_p\left(\frac{\partial T}{\partial t} + u\frac{\partial T}{\partial x} + v\frac{\partial T}{\partial y}\right) = k\frac{\partial^2 T}{\partial y^2} \tag{4}$$

$$\frac{\partial}{\partial t}\int_0^\Delta T\,dy - T_\infty\frac{\partial \Delta}{\partial t} + \frac{\partial}{\partial x}\int_0^\Delta u(T - T_\infty)\,dy = -\left.\frac{k}{\rho c_p}\frac{\partial T}{\partial y}\right|_{y=0} \tag{5}$$

With reference to the unsteady stagnation flow in Fig. 1, $\delta = \delta(x, t)$, $\Delta = \Delta(x, t)$, $u = u(x, y, t)$, $p = p(x, t)$, $U_\infty = U_\infty(x, t)$, and $T = T(x, y, t)$ in Eqs. (2–5).

The differential forms of the momentum and energy conservation equations [Eqs. (2) and (4)], and physically appropriate matching conditions which must be satisfied by specified expressions for $u(x, y, t)$ and $T(x, y, t)$, give the following:

Surface ($y = 0$)

$$u = 0 \tag{6a}$$

$$v = 0 \tag{6b}$$

$$\frac{\partial u}{\partial t} = 0 \tag{6c}$$

$$0 = -\frac{1}{\rho}\frac{\partial p}{\partial x} + \nu\frac{\partial^2 u}{\partial y^2} \tag{6d}$$

$$T = T_s \tag{7a}$$

$$\frac{\partial T}{\partial t} = \frac{\nu}{Pr}\frac{\partial^2 T}{\partial y^2} \tag{7b}$$

Edge of hydrodynamic boundary layer ($y = \delta$)

$$u = U_\infty(x, t) \tag{8a}$$

$$\frac{\partial u}{\partial y} = 0 \tag{8b}$$

$$\frac{\partial^2 u}{\partial y^2} = 0 \tag{8c}$$

Edge of thermal boundary layer ($y = \Delta$)

$$T = T_\infty \tag{9a}$$

$$\frac{\partial T}{\partial y} = 0 \tag{9b}$$

$$\frac{\partial^2 T}{\partial y^2} = 0 \tag{9c}$$

Beyond the hydrodynamic boundary layer ($y > \delta$), $u = U_\infty$ and the flow is governed by the time-dependent Euler equation below:

$$\frac{\partial U_\infty}{\partial t} + U_\infty \frac{\partial U_\infty}{\partial x} = -\frac{1}{\rho}\frac{\partial p}{\partial x} \tag{10}$$

Since $\partial p/\partial y << \partial p/\partial x$ across the velocity boundary layer, Eq. (10) relates the pressure gradient $\partial p/\partial x$ in Eqs. (2), (3), and (6d) to the freestream velocity U_∞.

Model Formulation

Physically correct and *temporally adaptive* polynomial profiles of fourth order were implemented to represent flow velocity and temperature across the hydrodynamic and thermal boundary layers. Transient effects are incorporated in the velocity profile by Eqs. (8a) and (10) coupled with Eq. (6d), and by temporal changes in the thickness of the hydrodynamic boundary layer. Similarly, transient effects are incorporated in the temperature profile through the energy balance in the fluid at the impingement surface given by Eq. (7b) and by temporal changes in the thickness of the thermal boundary layer. The influence of the hydrodynamic boundary-layer response on the transient thermal boundary-layer thickness is included via advective terms appearing in the energy conservation equation [Eq. (5)]. When subject to Eqs. (6–10), and expressed in dimensionless forms, the appropriate polynomials are given by Eqs. (11) and (12)

$$u_* = \left(2 + \frac{\Lambda\Omega}{6}\right)\eta - \frac{\Lambda\Omega}{2}\eta^2 + \left(\frac{\Lambda\Omega}{2} - 2\right)\eta^3 + \left(1 - \frac{\Lambda\Omega}{6}\right)\eta^4 \tag{11}$$

$$\Theta = \Theta_s - \left(2\Theta_s + \frac{\omega}{3}\right)\beta + \omega\beta^2 + (2\Theta_s - \omega)\beta^3 + \left(\frac{\omega}{3} - \Theta_s\right)\beta^4 \tag{12}$$

where

$$\Omega = \frac{1}{U_{\infty *}}\frac{\partial U_{\infty *}}{\partial \tau} + \frac{1}{C_*}\frac{\partial U_{\infty *}}{\partial x_*} \tag{13}$$

$$\omega = \Gamma\frac{Pr}{2}\frac{d\Theta_s}{d\tau} \tag{14}$$

Upon combining Eqs. (3), (10), and (11) and carefully observing functional dependencies, a partial differential equation for the hydrodynamic boundary layer $\delta(x, t)$ results in which explicit functions of the spatial variable x appear only as products with $\partial\delta/\partial x$. The symmetry in the dividing flow about the stagnation streamline and the associated spatial constancy of the hydrodynamic boundary layer ($\partial\delta/\partial x = 0$) is invoked to remove all such terms. An ordinary differential equation with t as the sole independent variable is thereby obtained and is given below in terms of Λ and τ:

$$\frac{d\Lambda}{d\tau}\frac{1}{20}\left[(\Omega_1 + \Omega_2)\frac{1}{4}\Lambda - 3\right] = -2 + \Psi_1\Lambda - \Psi_2\Lambda^2 - \Psi_3\Lambda^3 \tag{15}$$

where

$$\Omega_1 = \frac{1}{U_{\infty *}}\frac{\partial U_{\infty *}}{\partial \tau} \tag{16a}$$

$$\Omega_2 = \frac{1}{C_*}\frac{\partial U_{\infty *}}{\partial x_*} \tag{16b}$$

$$\Psi_1 = \tfrac{2}{15}\Omega_1 + \tfrac{116}{315}\Omega_2 \tag{17}$$

$$\Psi_2 = \tfrac{1}{120}\Omega_1^2 + \tfrac{71}{3780}\Omega_1\Omega_2 + \tfrac{79}{7560}\Omega_2^2 \tag{18}$$

$$\Psi_3 = \tfrac{1}{4536}(\Omega_1 + \Omega_2)^2\Omega_2 \tag{19}$$

The governing transient, ordinary differential equation for Θ_s is obtained from an energy balance at the surface, with the dimensionless temperature gradient $\partial\Theta/\partial\beta|_{\beta=0}$ in the fluid determined from Eq. (12)

$$q_s = -k\left.\frac{\partial T}{\partial y}\right|_{y=0} = -\frac{k}{\Delta}(T_{s_0} - T_\infty)\left.\frac{\partial\Theta}{\partial\beta}\right|_{\beta=0} \tag{20}$$

$$\frac{d\Theta_s}{d\tau} = \frac{6}{Pr\Gamma}(q_{s*}\Gamma^{1/2} - 2\Theta_s) \tag{21}$$

where q_{s*} is the imposed dimensionless heat flux at the surface and is defined by

$$q_{s*} = \frac{q_s}{k\sqrt{(C/\nu)}(T_{s_0} - T_\infty)} \tag{22}$$

With the condition $\partial\Delta/\partial x = 0$, Eqs. (5), (11), and (12) yield the ordinary differential equation for the time-dependent Γ:

$$\frac{d\Gamma}{d\tau}\left(4 - \frac{q_{s*}}{\Theta_s}\Gamma^{1/2}\right) = \frac{96}{Pr} - \Gamma^{1/2}\frac{28}{Pr}\frac{q_{s*}}{\Theta_s} - \Gamma^{3/2}f_1(\Lambda, \Theta_s) + \Gamma^2 f_2(\Lambda, \Theta_s) - \Gamma^{5/2}f_3(\Lambda, \Theta_s) - \Gamma^3 f_4(\Lambda, \Theta_s) + \Gamma^{7/2}f_5(\Lambda, \Theta_s) \tag{23}$$

where

$$f_1(\Lambda, \Theta_s) = 4\Omega_2\Lambda^{-1/2} + \frac{1}{3}\Psi_4\Lambda^{1/2} - \frac{1}{\Theta_s}\frac{dq_{s*}}{d\tau} \quad (24)$$

$$f_2(\Lambda, \Theta_s) = \tfrac{1}{5}[\tfrac{8}{9}\Psi_4 + (2\Omega_2\Lambda^{-1/2} + \tfrac{1}{6}\Psi_4\Lambda^{1/2})(q_{s*}/\Theta_s)] \quad (25)$$

$$f_3(\Lambda, \Theta_s) = \tfrac{1}{7}[\tfrac{5}{4}\Psi_4\Lambda^{-1/2} - 5\Omega_2\Lambda^{-3/2} + \tfrac{1}{2}\Psi_4(q_{s*}/\Theta_s)] \quad (26)$$

$$f_4(\Lambda, \Theta_s) = \tfrac{1}{7}\Lambda^{-1/2}\left\{\left[\tfrac{4}{3}\Lambda^{-1/2} + \left(\frac{q_{s*}}{\Theta_s}\right)\right]\Omega_2\Lambda^{-1} - \left[\tfrac{2}{9}\Lambda^{-1/2} + \frac{1}{4}\left(\frac{q_{s*}}{\Theta_s}\right)\right]\Psi_4\right\} \quad (27)$$

$$f_5(\Lambda, \Theta_s) = \tfrac{5}{126}(q_{s*}/\Theta_s)\Lambda^{-1}(\Omega_2\Lambda^{-1} - \tfrac{1}{6}\Psi_4) \quad (28)$$

$$\Psi_4 = (\Omega_1 + \Omega_2)\Omega_2 \quad (29)$$

The convective heat transfer coefficient is obtained from Newton's law of cooling and Eq. (20):

$$h = \frac{-k\left.\frac{\partial T}{\partial y}\right|_{y=0}}{T_s - T_\infty} = \frac{-k\left.\frac{\partial \Theta}{\partial \beta}\right|_{\beta=0}}{\Theta_s \Delta} \quad (30)$$

With the temperature gradient at the surface obtained from Eqs. (12) and (14), Nusselt number is given by

$$Nu_w = \frac{w}{\sqrt{\Gamma}}\sqrt{(C/\nu)}\left(2 + \frac{\Gamma Pr}{6\Theta_s}\frac{d\Theta_s}{d\tau}\right) \quad (31)$$

The dimensionless variables q_{s*} [Eq. (22)] and Θ_s [Eq. (21)] depend only on τ, and Nu_w is thereby spatially constant, as expected in the stagnation region. In order to assess whether time-averaged heat transfer is affected, a time-averaged Nusselt number is defined in Eq. (32) which is referenced to the corresponding steady-state value. Equation (32) is based on an instantaneous energy balance at the surface and thereby gives results equivalent to what would be measured experimentally. No influence on heat transfer is indicated when $Nu_{*,avg} = 1$. Integration was performed over a large number n of pulsation periods $1/f_*$ to ensure accuracy to within the smallest decimal place in all reported values:

$$Nu_{*,avg} = \left(\int_0^{n/f_*} Nu_*\Theta_s\, d\tau \Big/ \int_0^{n/f_*} \Theta_s\, d\tau\right) \quad (32)$$

Forcing Functions for Flow and Surface Heat Flux

An important advantage of the present model is that boundary-layer behavior can be predicted for any specified temporal variation in the freestream velocity $U_{\infty *}(x_*, \tau)$ $(= U_\infty/V_{i0})$ in Eq. (8a) or surface heat flux $q_{s*}(\tau)$ in Eq. (22), as long as the variations are piecewise smooth. Since the precise characteristics of temporal flow variations are dependent on specific physical circumstances, the general features of Eq. (1) for steady stagnation flow were assumed to apply so as to obtain forcing functions which converge on the steady flow case as forcing frequencies approach zero. Therefore, transient terms were introduced by assuming that the dimensionless velocity gradient C_* from potential flow theory remains unchanged and that unsteadiness in the incident velocity $V_i(t)$ (Fig. 1) induces temporal variations in the dimensional velocity gradient C_i. The influences of the flow characteristics and surface heat flux variations are assessed by considering responses to two otherwise unique forcing functions for $U_{\infty *}(x_*, \tau)$ and $q_{s*}(\tau)$. Sinusoidal forcing functions were specified about initial, steady-state values and are given in Eqs. (33) and (34) with $0 < \varepsilon_1 < 1$ and $0 < \varepsilon_2 < 1$ by

$$u_*(\tau) = C_* x_*[1 + \varepsilon_1 \sin(2\pi f_* \tau)] \quad (33)$$

$$q_{s*}(\tau) = q_{s,0*}[1 + \varepsilon_2 \sin(2\pi f_{q*}\tau)] \quad (34a)$$

where

$$q_{s0*} = (2/\sqrt{\Gamma_0}) \quad (34b)$$

Solution Methodology and Model Verification

Steady-state values Λ_0, Γ_0, and q_{s0*} were determined from Eqs. (15), (21), and (23) with all time-derivatives set to zero and $\Theta_s = \Theta_{s0} = 1$. The secant method[20] was used to solve

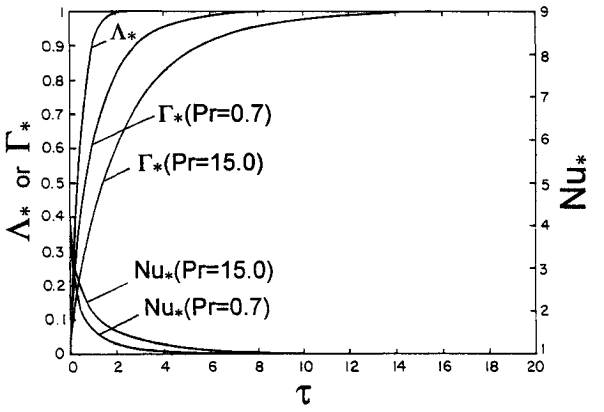

Fig. 2 Unforced transient responses of the hydrodynamic and thermal boundary-layer thicknesses and Nusselt number with $Nu_{w0}/w\sqrt{C/\nu}(Pr = 0.7) = 0.5008$, $Nu_{w0}/w\sqrt{C/\nu}(Pr = 15) = 1.5823$, $\Gamma(\tau = 0) = 0$, $\Gamma_0(Pr = 0.7) = 15.9513$, $\Gamma_0(Pr = 15) = 1.5977$, $\Theta(\tau = 0) = 0$, $\Lambda(\tau = 0) = 0$, and $\Lambda_0 = 7.052324$.

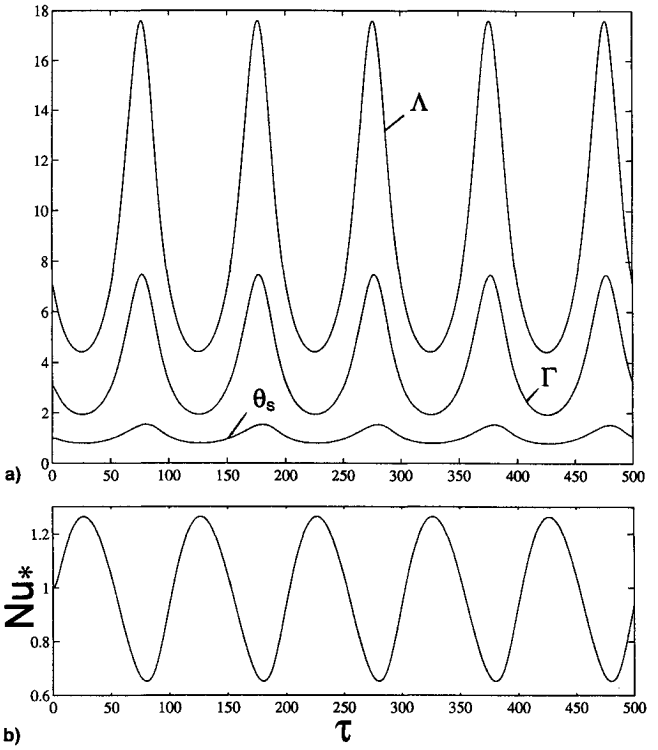

Fig. 3 Response due to sinusoidal flow pulsations [Eq. (32)] and steady surface heat flux ($\varepsilon_2 = 0$) with $f_* = 0.01$, $\varepsilon_1 = 0.60$, $Pr = 6$, $Nu_{w0}/w\sqrt{C/\nu}(Pr = 6) = 1.1378$, and $\Gamma_0(Pr = 6) = 3.0896$: a) dimensionless boundary-layer thicknesses and surface temperature and b) Nusselt number.

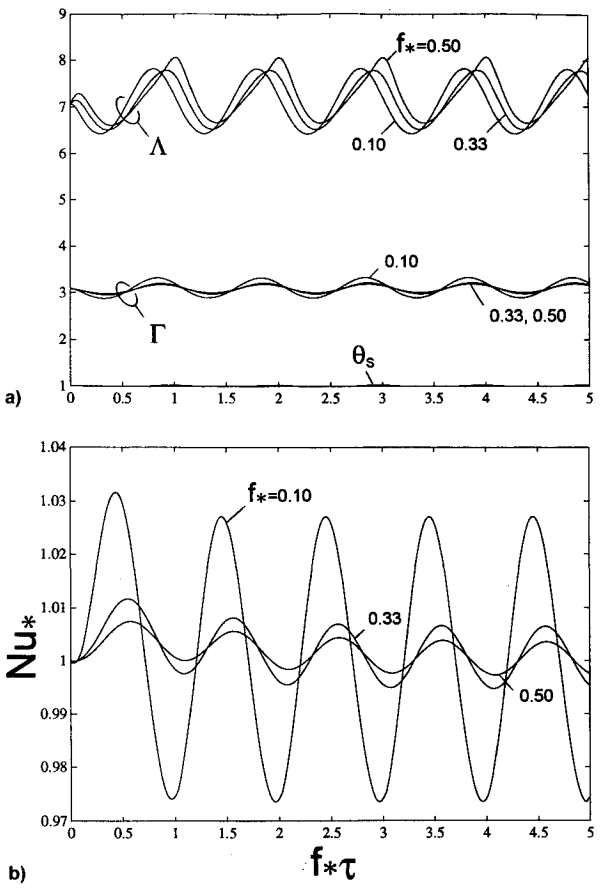

Fig. 4 Influence of frequency on the response due to sinusoidal flow pulsations [Eq. (32)] for a constant surface heat flux ($\varepsilon_2 = 0$) with $\varepsilon_1 = 0.10$, $Pr = 6$, $Nu_{w0}/w\sqrt{C/\nu}(Pr = 6) = 1.1378$, and $\Gamma_0(Pr = 6) = 3.0896$: a) dimensionless boundary-layer thicknesses and surface temperature and b) Nusselt number.

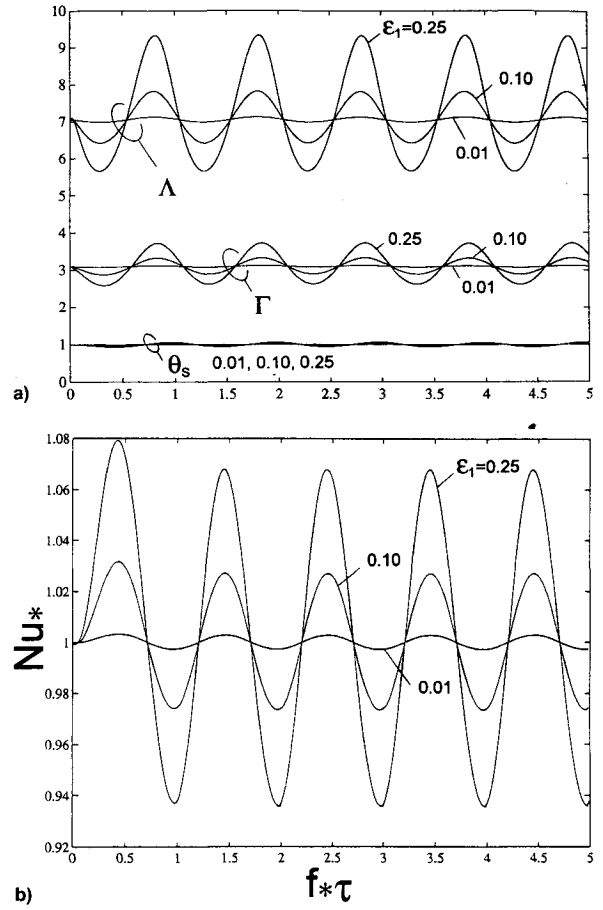

Fig. 5 Influence of amplitude ε_1 on the response due to sinusoidal flow pulsations [Eq. (32)] for a constant surface heat flux ($\varepsilon_2 = 0$) with $f_* = 0.1$, $Pr = 6$, $Nu_{w0}/w\sqrt{C/\nu}(Pr = 6) = 1.1378$, and $\Gamma_0(Pr = 6) = 3.0896$: a) dimensionless boundary-layer thicknesses and surface temperature and b) Nusselt number.

the resulting nonlinear equations to within a convergence tolerance 10^{-6}. Runge-Kutta algorithms were implemented to obtain numerical solutions to the three ordinary, nonlinear equations differential equations for Λ, Θ_s, and Γ. Variable dimensionless time steps were incorporated in the algorithms to reduce computational time, because calculations sometimes extended over several thousand periods of the forcing functions in order to illuminate the nonlinear dynamic response. Beginning time steps were selected as small fractions of the *unforced response time* (see below) or of the forcing function period. Maximum time steps were controlled and were successively halved until differences in successive computations were within a tolerance of 10^{-6}. In addition, both fourth-order and fifth-order Runge-Kutta algorithms were used to ensure algorithm-independence in the calculated results. Power spectral densities were determined from results calculated with constant time steps equal to the smallest time step encountered in the respective solution with the variable time step approach.

The model was verified by comparison under steady-state conditions to known analytical solutions, and under transient conditions to experimental results for stagnation flows about cylinders and spheres. Values of Λ_0 and Γ_0 were identical to those reported by Zumbrunnen,[9] and calculated Nusselt numbers were determined to be within 1–2.3% of those obtained from the similarity solutions for flow past a wedge.[21] Van der Hegge Zijnen[22] reported that Nusselt numbers for a 0.005-mm-diam tungsten wire in an air crossflow decreased up to 4.3% when the wire was vibrated with amplitudes up to 45% of the flow velocity. A similar study was performed later by Sreenivasan and Ramachandran.[23] Experimental correlations were developed in both studies. Results for Nu_w with constant surface heat flux and sinusoidal flow variations agree to within 1% of both experimental correlations for flow variations within the range of the correlations (i.e., $f < 47$ Hz).

Results and Discussion

Equations (15), (21), and (23) constitute a nonautonomous system of three coupled, nonlinear, ordinary differential equations which govern the transient responses of the hydrodynamic and thermal boundary layers and surface temperature in terms of the variables Λ, Γ, and Θ_s. When taken together with the forcing functions for incident flow velocity and surface heat flux given by Eqs. (33) and (34), solutions in terms of τ are dependent on the parameters Pr, C_*, ε_1, ε_2, f_*, and f_{q^*}. The responses are strongly influenced in dimensional terms by C. Freestream velocity gradients are smaller in stagnation flows with larger characteristic dimensions, and the hydrodynamic and thermal boundary layer responses are thereby less rapid for impinging jets with larger widths or for cylinders, turbine blades, or sensor bodies in a crossflow with larger diameters or chord sizes. Values of C for cylinders and planar jets[9] may be used to convert the scaled or dimensionless results presented in this study to dimensional values for specific applications.

Before proceeding with the boundary-layer dynamics and transient heat transfer due to temporal changes in the incident flow velocity and/or surface heat flux, it is of interest to consider the *unforced response* of Eqs. (15) and (23) to ascertain the boundary-layer behavior with no applied external stimulus. For the unforced response shown in Fig. 2, constant flow and surface heat flux are specified ($\varepsilon_1 = 0$; $\varepsilon_2 = 0$) and both Λ and Γ are initially assigned values of zero. [To avoid singularities at $\tau = 0$, integration was performed initially with limiting representations of Eqs. (15) and (23) as $\Lambda, \Gamma \to 0$.[24]]

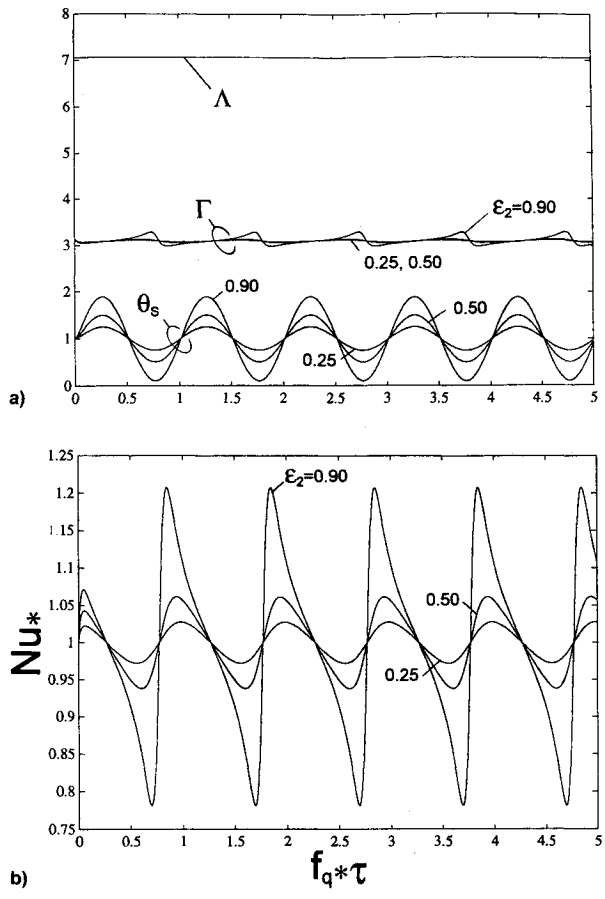

Fig. 6 Influence of the amplitude ε_2 on the response due to sinusoidal heat flux pulsations [Eq. (33)] for steady flow ($\varepsilon_1 = 0$) with $f_{q*} = 0.01$, $Pr = 6$, $Nu_{w0}/w\sqrt{C/\nu}(Pr = 6) = 1.1378$, and $\Gamma_0(Pr = 6) = 3.0896$: a) dimensionless boundary-layer thicknesses and surface temperature and b) Nusselt number.

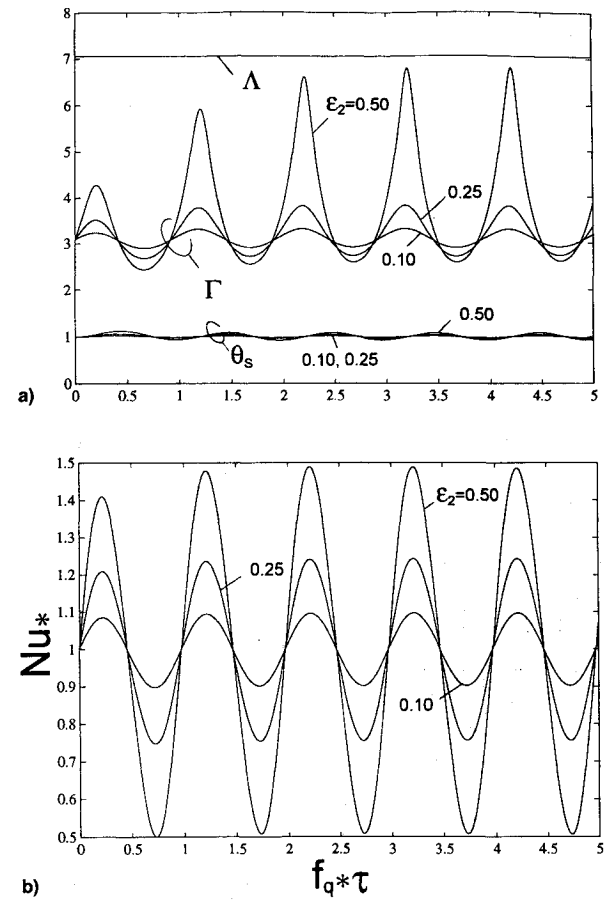

Fig. 7 Influence of the amplitude ε_2 on the response due to sinusoidal heat flux pulsations [Eq. (33)] for steady flow ($\varepsilon_1 = 0$) with $f_{q*} = 0.8$, $Pr = 6$, $Nu_{w0}/w\sqrt{C/\nu}(Pr = 6) = 1.1378$, and $\Gamma_0(Pr = 6) = 3.0896$: a) dimensionless boundary-layer thicknesses and surface temperature and b) Nusselt number.

The thermal boundary-layer response in terms of Γ lags the hydrodynamic boundary layer in terms of Λ. Corresponding Nusselt numbers Nu_w relative to the steady-state value Nu_{w0} were calculated from Eq. (31). As boundary-layer development proceeds ($\Lambda_*, \Gamma_* \rightarrow 1$), the ratio Nu/Nu_0 approaches the steady-state value of unity. Thermal boundary-layer development is more rapid for $Pr = 0.7$ than for $Pr = 15$, since heat is transferred more readily in fluids with higher thermal diffusivities.

The transient responses of Λ, Γ, Θ_s and Nu_* due to the sinusoidal variation in the incident flow velocity given by Eq. (33) are shown in Fig. 3 for a constant surface heat flux ($\varepsilon_2 = 0$) with $Pr = 6.0$, $f_* = 0.01$, and $\varepsilon_1 = 0.60$. (In all figures which follow, responses begin from steady-state conditions.) Responses for $0 < f_* < 0.06$ and $0 < \varepsilon_1 < 0.60$ were qualitatively similar, since the responses of both boundary layers are sufficiently rapid to follow the dynamics of the incident flow velocity when the disturbance periodicity is much greater than the durations for the unforced time responses in Fig. 2. Nusselt numbers in Fig. 3b become larger during periods of decreasing boundary-layer thickness, and smaller during periods of increasing boundary-layer thickness. Time-averaged values of Λ and Γ increase by about 30%, and the time-averaged Nu_w [Eq. (33)] decreases by about 7.3%. Experimental work[2] reported recently found that time-averaged stagnation line Nusselt numbers for a pulsating planar water jet impinging on a constant heat flux surface decreased with pulsation frequency. Experimentally determined decreases, which were not influenced by distortions in the jet free surface, agree to within 2% of the model predictions. Thus, nonlinear dynamical effects might be utilized to reduce heat transfer to surfaces, such as frontal regions of gas turbine blades, exposed to a periodic stagnation flow.

In Fig. 4, as f_* is raised, an initial transient becomes evident over the first two cycles, and nonlinearities cause the responses to become markedly different from those in Fig. 3 at low frequencies. The response for Λ diverges from sinusoidal; however, Nusselt numbers beyond the initial transient deviate equally about the steady-state value ($Nu_w/Nu_{w0} = Nu_* = 1$). In Fig. 5, as the magnitude ε_1 for the incident sinusoidal flow variation increases with $f_* = 0.1$, maximal departures from mean values become greater and corresponding time-averaged Nusselt numbers increase by less than 2%. Thus, small enhancements are predicted for high-frequency pulsations.

Results pertaining to the sinusoidal surface heat flux variation [Eq. (34)] and steady flow ($\varepsilon_1 = 0$) are shown in Fig. 6. The hydrodynamic boundary-layer thickness $\Lambda = \Lambda_0 = 7.052324$ in the steady flow. Departures in the thermal boundary-layer thickness from steady state remain small even as the magnitude ε_2 of the heat flux variation increases from 0.25 to 0.90. Small departures occur since the dimensionless period for the variations ($f_{q*}^{-1} = 100$) is much larger than the duration of the unforced time response in Fig. 2. However, variations in the surface heat flux affect preferentially the temperature gradient in fluid layers near the surface, yielding more significant variations in Θ_s and Nu_w. Interestingly, for $\varepsilon_2 = 0.50$ and $\varepsilon_2 = 0.90$, decreases in Nusselt numbers occur more slowly than do increases. The simple periodic response for Θ_s reflects the linearity of the energy equation in terms of temperature, as expected. Although not presented, calculations were performed in the range $0.01 < f_{q*} < 0.10$, and qualitatively similar responses were found. For $f_{q*} > 0.10$, the responses of Fig. 6 marked by different behavior during increasing and decreasing Nusselt number no longer occurred. Results for these conditions are given in Fig. 7. For these

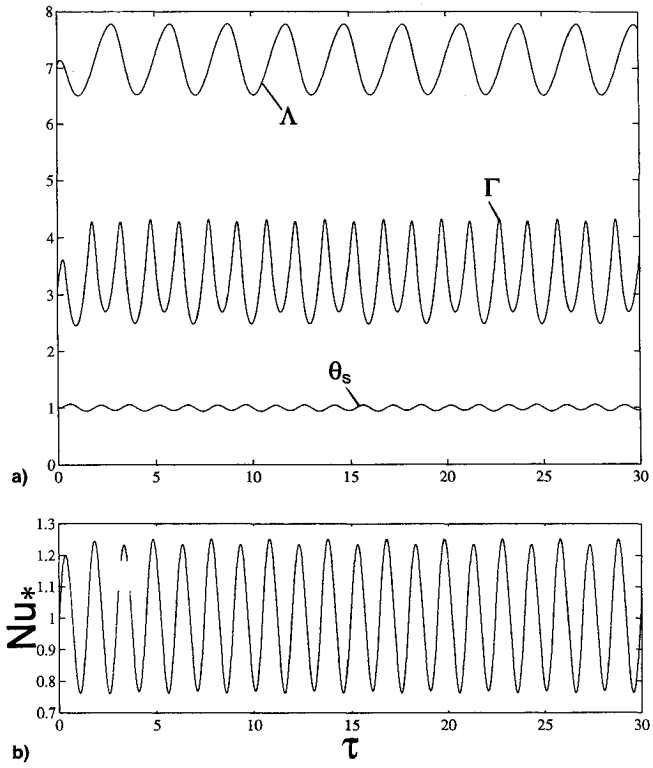

Fig. 8 Response due to simultaneous sinusoidal flow and surface heat flux pulsations with $f_* = \frac{1}{3}$, $\varepsilon_1 = 0.10$, $f_{q*} = 0.67$, $\varepsilon_2 = 0.25$, $Pr = 6$, $Nu_{w0}/w\sqrt{C/\nu}(Pr = 6) = 1.1378$, and $\Gamma_0(Pr = 6) = 3.0896$: a) dimensionless boundary-layer thicknesses and surface temperature and b) Nusselt number.

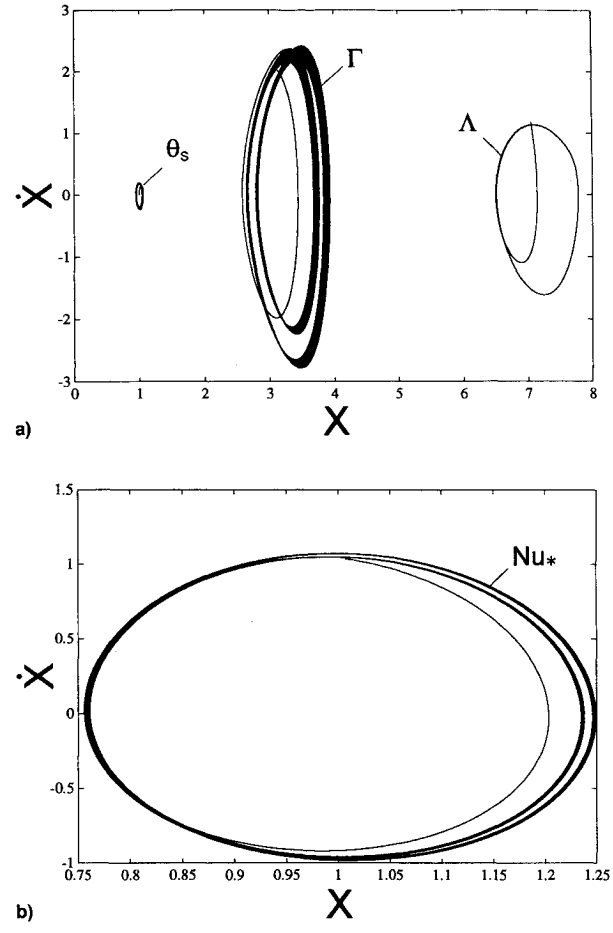

Fig. 9 Phase portraits for the conditions in Fig. 8: a) dimensionless boundary-layer thicknesses and surface temperature and b) Nusselt number.

higher dimensionless frequencies, the rapidity of the surface heat flux variations greatly exceeds the unforced response time for Γ (Fig. 2) and departures from the steady-state value Γ_0 are thereby larger than in Fig. 6. Moreover, the mean value of Γ increases with ε_2. Following an initial transient ($0 < \tau < 2$), the thermal boundary-layer dynamics lead to sinusoidal variations in Nu_w with peak deviations from the initial steady-state value Nu_{w0} comparable to ε_2.

Responses when the incident freestream velocity and surface heat flux simultaneously vary according to Eqs. (33) and (34) were studied systematically over the parametric ranges $0.7 < Pr < 15$, $0.01 < f_* < 0.40$, $0.33 < f_{q*}/f_* < 4$, $0.06 < \varepsilon_1 < 0.6$, and $0.1 < \varepsilon_2 < 0.9$. In all cases, the Prandtl number had little effect on the nature of the thermal boundary layer and Nusselt number responses. As oscillation amplitudes ε_1 and ε_2 were raised above 30%, the time-averaged boundary-layer thicknesses increased, but increases became progressively smaller and limiting values were approached. The time-averaged Nusselt number remained close to its steady-state value ($Nu_{*,\mathrm{avg}} = 1$). When the forcing frequencies f_* and f_{q*} were varied within the ranges above, $Nu_{*,\mathrm{avg}}$ also remained close to unity. However, the instantaneous responses differed markedly, owing to nonlinearities in the governing equations. Results exhibited a strong sensitivity to the ratio $m = f_*/f_{q*}$ of the two forcing frequencies. When the frequency ratio m was an integer, periodical behavior ensued with a waveform consisting of m principal frequencies. When m was rational, the number of principal frequencies equalled the integer closest to m and various secondary frequencies accompanied each component frequency. This type of response is often called *multiperiodic*. When by contrast m was irrational, the number of secondary frequencies increased considerably. The forcing frequencies in this case are said to be *incommensurate*, and the response is referred to as *quasiperiodic* since the principal frequencies remain distinctive even as the number of secondary frequencies become larger. However, when the frequencies are incommensurate, the frequency spectrum broadening may become more pronounced as a parameter is altered, and chaotic behavior may result.[25] Two particular cases were chosen to illustrate complex and qualitatively different responses. Due to the complexity of the solutions, results are expressed in terms of phase portraits, Poincaré maps and Fourier spectra in addition to the temporal variations. It should be noted that the set of irrational numbers is larger than the set of rational numbers. Thus, quasiperiodic behavior is not an unlikely condition in doubly forced systems.

The dynamics for $Pr = 6$, $f_* = 0.33$, $\varepsilon_1 = 10\%$, $f_{q*}/f_* = 2.01$, and $\varepsilon_2 = 25\%$ are presented in Figs. 8–10. Results for Prandtl numbers of 0.7 and 15 were qualitatively similar under identical conditions. The Λ in Fig. 8a follows the dynamics of the flow velocity with a phase delay of one-half cycle. Although not shown, similar responses were obtained for C_{f*}. In Figs. 8a and 8b, two major frequencies which correspond to f_* and f_{q*} can be noticed in the temporal variations of Γ and Nu_*. The time-averaged surface temperature and Nusselt number remain close to their steady-state values ($\Theta_s = 1$ and $Nu_* = 1$), even though the time-averaged value of Γ increases by about 1%. The thermal boundary layer and Nusselt number variations lag the surface temperature response which has a comparatively small amplitude. For the sake of clarity, the phase portraits presented here include only sufficient results to depict the nature of individual trajectories. The phase portrait of Λ in Fig. 9a shows a closed orbit with a very short starting transient spanning less than two cycles of the forcing function for U_∞. (Starting transients in the phase portraits have been retained to exhibit the trajectory from the initial, steady-state conditions.) The simple orbit arises since the momentum equation is uncoupled to the energy equation with the assumption of constant thermophysical properties invoked in the analysis. When the response of a dependent variable

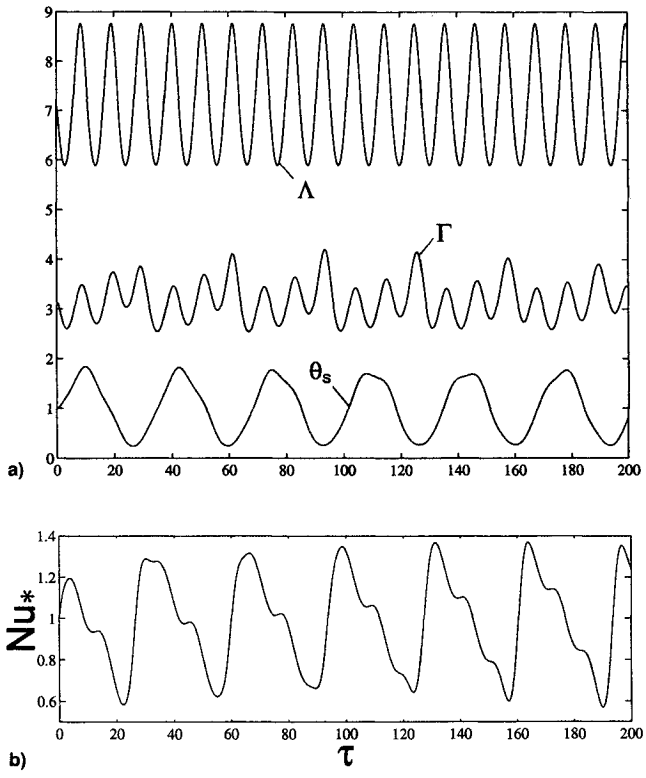

Fig. 10 Response due to simultaneous sinusoidal flow and surface heat flux pulsations with $f_* = 0.0942$, $\varepsilon_1 = 0.20$, $f_{q*} = 0.03$, $\varepsilon_2 = 0.80$, $Pr = 6$, $Nu_{w0}/w\sqrt{C/\nu}(Pr = 6) = 1.1378$, and $\Gamma_0(Pr = 6) = 3.0896$: a) dimensionless boundary-layer thicknesses and surface temperature and b) Nusselt number.

is influenced by two forcing functions of different frequencies, as for Γ, Θ_s, and Nu_*, the *motion* in a phase plane appears to take place on the surface of a torus [doughnut-shaped figure].[25] Because the ratio f_*/f_{q*} of the two forcing frequencies is a rational number in Fig. 9, it is expected that the trajectory on the torus will close and thereby repeat. A simple torus is evident in Figs. 9a and 9b, where two major loops of the torus correspond to the two forcing frequencies and individual orbits within each major loop reveal the existence of secondary periodicities.

In order to further characterize the dynamic behavior given in Fig. 8, a time series was constructed of the peak values of Γ. The successive value Γ_{n+1} in the series was then plotted against the previous value Γ_n. Such a plot, known as a *first-return map*, is a type of Poincaré map and depicts periodic motion as a finite number of points. For example, a pure sine wave response of amplitude one would yield a single point at $(x, y) = (1, 1)$, whereas a chaotic response yields an unbounded number of points as time approaches infinity which may form a fractal structure. Each point in a Poincaré map would correspond to a distinct orbit in the phase portrait for Γ (Fig. 9a). Although not shown, a Poincaré map was constructed for Γ in Fig. 9a which consisted of a set of points forming a very narrow loop, twisted once near $\Gamma_n = 3.7$, and nearly symmetric about the main diagonal ($\Gamma_n = \Gamma_{n+1}$). Thus, at each Γ_n, the loop yielded two possible future values Γ_{n+1}, revealing some small unpredictability in the system history. The power spectral density (PSD) for $\Gamma(\tau)$ revealed discrete frequencies at the principal forcing frequencies f_* and f_{q*} and their related harmonics. Although complex with some degree of unpredictability, the response may be classified as multiperiodic.

Quasiperiodic behavior is of interest here since it is a known route to chaotic response and since incommensurate frequencies in doubly forced systems are not unlikely (see above). A very complex response due to quasiperiodic behavior with $Pr = 6$, $f_* = 0.09$, $\varepsilon_1 = 20\%$, $f_{q*}/f_* = 1/\pi$ and $\varepsilon_2 = 80\%$

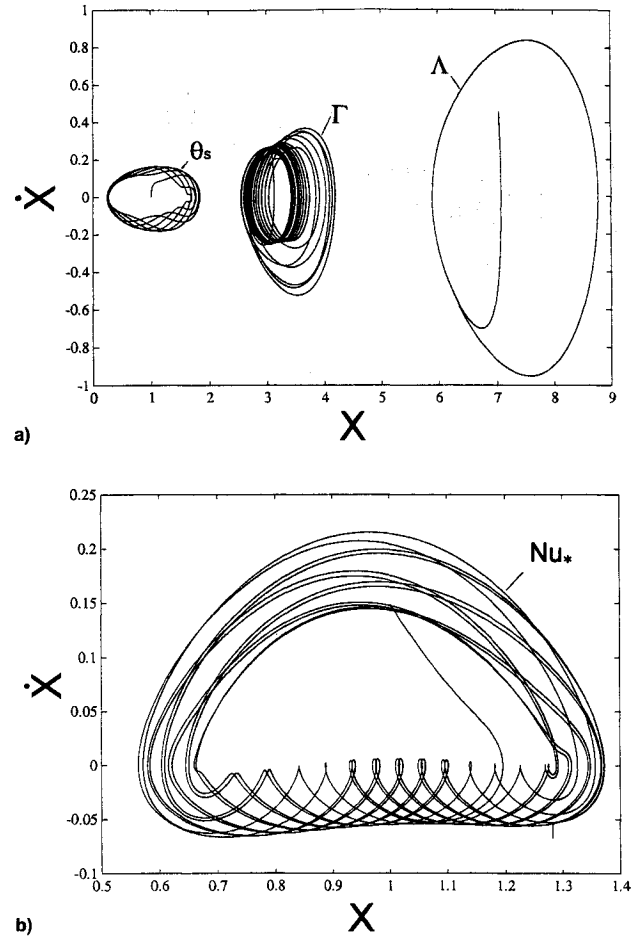

Fig. 11 Phase portraits for the conditions in Fig. 10: a) dimensionless boundary-layer thicknesses and surface temperature and b) Nusselt number.

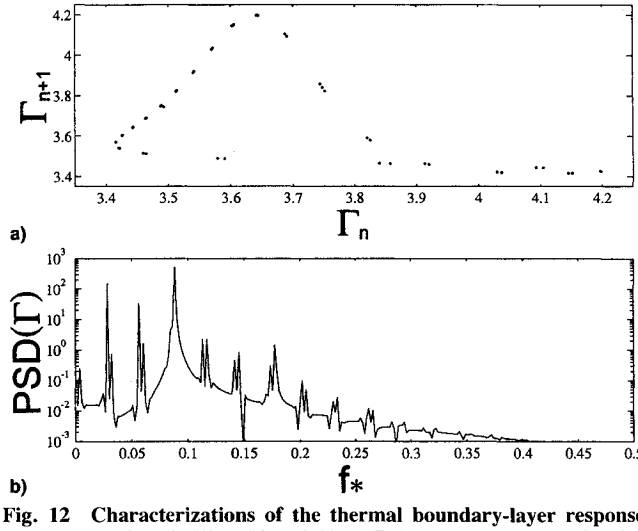

Fig. 12 Characterizations of the thermal boundary-layer response for the conditions in Figs. 10 and 11: a) Poincaré map and b) Fourier spectrum.

is shown in Figs. 10–12. Unlike conditions for Figs. 8 and 9, the frequency for the flow variation is larger than the frequency for the surface heat flux variation, and the amplitude of the flow variation is smaller. Responses in Fig. 10 for Γ, Θ_s, and Nu_* are more complex and variable than those in Fig. 8; however, the response for Λ is qualitatively similar. The time-averaged surface temperature and Nusselt number remain close to their steady-state values ($\Theta_s = 1$ and $Nu_* = 1$), even though the time-averaged value of Γ increases by about 4%. The trajectories in the phase portraits of Fig. 11

reveal greater frequency content in the response. Noteworthy is that the response patterns differ for each variable: Λ—a single periodic orbit; Γ—a variable diameter coil with orbits most frequently at the smaller diameters; Θ_s—a torus; Nu_*—a combination torus and coil. Comparison of Figs. 9 and 11 reveals that the torus structure in the phase portraits, which is a characteristic of multiperiodic and quasiperiodic responses, degenerates and leads to spurious trajectories in Fig. 11. The Poincaré map is shown in Fig. 12a. Its lack of symmetry around the main diagonal ($\Gamma_{n+1} = \Gamma_n$) indicates that trajectories calculated with forward time steps differ from those calculated with backward time steps. Thus, it is increasingly difficult to predict past behavior from a current condition. In Fig. 12b, the Fourier spectrum of Γ includes a multitude of frequencies other than the forcing frequencies f_* and f_{a*} or their harmonics. This broadening frequency content and the Poincaré map in Fig. 12a points to increasing complexity in the response. Hence, the dynamics of Γ, Θ_s, and Nu_* are tending towards unpredictability. However, the response is nonchaotic since the largest Lyapunov exponent was found to be -0.9862. A negative Lyapunov exponent is consistent with the closed loop in Fig. 12a and indicates insufficient sensitivity to initial conditions for chaotic behavior. If such complex behavior is encountered in a thermal sensor application, intervention by associated electronic control circuits may prove ineffective and lead to a chaotic response. A return to a simpler periodic response might be achieved through recently developed techniques in which details of the Poincaré map are used to determine conditions when a system can be nudged from a chaotic response by altering effective parameters or by selectively exciting dependent variables.[26] Moreover, since chaotic responses are comprised of a continuum of simpler unstable periodic responses, it is suggested that convective heat transfer might be favorably altered by causing a system to follow preferred orbits in phase space. A theoretical basis for this suggestion has been recently established.[27] The model developed in this study can be used to assess the viability of such approaches.

Conclusions

A detailed semianalytical model was developed to study the nonlinear dynamics of laminar boundary layers in a planar stagnation region due to temporal variations in the surface heat flux and incident flow velocity. Model predictions are in excellent agreement with reported experimental heat transfer results. For the sinusoidal variations imposed in this study, results indicate that instantaneous hydrodynamic and thermal boundary-layer thicknesses and Nusselt numbers deviate significantly from steady-state values. Markedly different instantaneous responses arise due to the influence of nonlinearities. Very complex excursions in convective heat transfer coefficients may be caused by an interaction between variations in the flow and imposed changes in surface heating. Over the ranges in parameters investigated, sinusoidal variations in the incident flow velocity induce decreases in time-averaged Nusselt numbers which might prove useful in reducing heat transfer to gas turbine blades exposed in situ to time-varying flows. Small increases in time-averaged Nusselt number occur at higher frequency pulsations of small amplitude. This result suggests that nonlinear dynamical effects enhance heat transfer in turbulent stagnation flows.

Acknowledgments

Support for this work was provided by the U.S. National Science Foundation under Grant CTS-8918154 and is gratefully acknowledged. The authors express their appreciation to Hussain Sheriff for assisting with model calculations.

References

[1]Zumbrunnen, D. A., and Aziz, M., "Convective Heat Transfer Enhancement Due to Intermittency in an Impinging Jet," *Journal of Heat Transfer*, Vol. 115, No. 1, 1993, pp. 91–98.

[2]Sheriff, H., and Zumbrunnen, D. A., "Effect of Flow Pulsations on the Cooling Effectiveness of an Impinging Water Jet," *Proceedings of the 29th National Heat Transfer Conference*, American Society of Mechanical Engineers, HTD Vol. 249, 1993, pp. 11–21; also *Journal of Heat Transfer* (to be published).

[3]Parker, T. S., and Chua, L. O., *Practical Numerical Algorithms for Chaotic Systems*, Springer-Verlag, New York, 1989, pp. 1–56.

[4]Saltzman, B., "Finite Amplitude Free Convection as an Initial Value Problem," *Journal of the Atmospheric Sciences*, Vol. 19, No. 4, 1962, pp. 329–341.

[5]Lorenz, E. N., "Deterministic Non-Periodic Flow," *Journal of the Atmospheric Sciences*, Vol. 20, March 1963, pp. 130–141.

[6]Erhard, P., Karcher, C., and Muller, U., "Dynamical Behavior of Natural Convection in a Double-Loop System," *Experimental Heat Transfer*, Vol. 2, No. 1, 1989, pp. 13–26.

[7]Weiss, N. O., "Dynamics of Convection," *Proceedings of the Royal Society of London*, Vol. A 413, No. 1, 1987, pp. 71–85.

[8]Rizwan-Uddin, and Dorning, J. J., "A Chaotic Attractor in a Periodically Forced Two-Phase Flow System," *Nuclear Science and Engineering*, Vol. 100, Dec. 1988, pp. 393–404.

[9]Zumbrunnen, D. A., "Transient Convective Heat Transfer in Planar Stagnation Flows with Time-Varying Surface Heat Flux and Temperature," *Journal of Heat Transfer*, Vol. 114, No. 1, 1992, pp. 85–93.

[10]Kasza, K. E., "Thermal Response Characteristics of Unsteady Stagnation Point Flows: A New Approach," *International Journal of Heat and Mass Transfer*, Vol. 18, No. 2, 1975, pp. 329–331.

[11]Andraka, C. E., and Diller, T. E., "Heat-Transfer Distribution Around a Cylinder in Pulsating Crossflow," *Journal of Engineering for Gas Turbines and Power*, Vol. 107, Oct. 1985, pp. 976–982.

[12]Rosiczkovski, J., and Hollworth, B., "Local and Instantaneous Heat Transfer from an Isothermal Cylinder Oscillating in a Cross-Flow," American Society of Mechanical Engineers, HTD Vol. 179, 1991, pp. 49–56.

[13]Schlichting, H., *Boundary-Layer Theory*, 7th ed., McGraw-Hill, New York, 1979, pp. 95–99, 206–217.

[14]Inada, S., Miyasaka, Y., and Izumi, R., "A Study of the Laminar Flow Heat Transfer Between a Two-Dimensional Water Jet and a Flat Surface with Constant Heat Flux," *Bulletin of the JSME*, Vol. 24, No. 196, 1981, pp. 1803–1810.

[15]Kuethe, A. M., and Schetzer, J. D., *Foundation of Aerodynamics*, Wiley, New York, 1959.

[16]Zumbrunnen, D. A., Incropera, F. P., and Viskanta, R., "A Laminar Boundary Layer Model of Heat Transfer Due to a Non-uniform Jet Impinging on a Moving Plate," *Warme-und Stoffubertragung*, Vol. 27, No. 1, 1992, pp. 311–319.

[17]Hansen, A. G., *Similarity Analysis of Boundary Value Problems*, Prentice-Hall, Englewood Cliffs, NJ, 1964.

[18]Boyd, J. P., *Lecture Notes in Engineering: Chebyshev and Fourier Spectral Methods*, Vol. 49, Springer-Verlag, Berlin, 1989.

[19]Dorning, J. J., "Nonlinear Dynamics and Chaos in Heat Transfer and Fluid Flow," AIChE Symposium Series-No. 269, Vol. 85, 1989.

[20]Gerald, C. F., *Applied Numerical Analysis*, Addison-Wesley, Reading, MA, 1978, pp. 11–13.

[21]Evans, H. L., "Mass Transfer Through Laminar Boundary Layers. 7. Further Similar Solutions to the B-Equation for the Case B = 0," *International Journal of Heat and Mass Transfer*, Vol. 5, No. 1, 1962, pp. 35–37.

[22]Van der Hegge Zijnen, B. G., "Heat Transfer from Horizontal Cylinders to a Turbulent Air Flow," *Applied Scientific Research*, Sec. A, Vol. 7, 1958, pp. 205–223.

[23]Sreenivasan, K., and Ramachandran, A., "Effect of Vibration on Heat Transfer from a Horizontal Cylinder to a Normal Air Stream," *International Journal of Heat and Mass Transfer*, Vol. 3, No. 1, 1961, pp. 60–67.

[24]Arpaci, S. V., and Larsen, P. S., *Convection Heat Transfer*, Prentice-Hall, Englewood Cliffs, NJ, 1984, pp. 277–286.

[25]Moon, F., *Chaotic Vibrations*, Wiley, New York, 1987.

[26]Garfinkel, A., Spano, M. L., Ditto, W. L., and Weiss, J. N., "Controlling Cardiac Chaos," *Science*, Vol. 257, Aug. 1992, pp. 1230–1235.

[27]Ott, E., Grebogi, C., and Yorke, J. A., "Controlling Chaos," *Physical Review Letters*, Vol. 64, No. 11, 1990, pp. 1196–1199.